Journal of Structural Geology, Vol. 12, No. 1, pp. 123 to 129, 1990
Printed in Great Britain

0191-8141/90 $3.00 + 0.00

Effect of mechanical interaction on the development of strike-slip faults with echelon patterns

ATILLA AYDIN and RICHARD A. SCHULTZ*

Rock Fracture Project, Department of Earth and Atmospheric Sciences, Purdue University, West Lafayette, IN 47907, U.S.A.

(*Received* 9 *December* 1988; *accepted in revised form* 23 *May* 1989)

Abstract—The overlapping geometry of echelon strike-slip faults is well-known. We have quantified this observation by measuring the amount of overlap and separation, and plotting them against each other for over 120 examples. Although there is large scatter, the data show a linear trend suggesting that the overlap increases proportionally with separation, up to a limiting value. We have analyzed this conspicuous relationship in terms of fault interaction by using a numerical model based on displacement discontinuity. The results show that fault interaction is, in fact, an important factor in contributing to the overlapping geometry of echelon strike-slip faults.

INTRODUCTION

IT IS well known that map traces of strike-slip faults are characteristically discontinuous and fault segments or strands are non-colinear (Wallace 1973, Bonila 1979, Sharp 1979, Allen 1981). Adjacent discrete segments step aside and overlap slightly to form what is commonly known as an echelon fault geometry. This conspicuous fault geometry is quite common not only on the Earth, but also on Mars (Schultz in press). There has been an increasing number of studies on the nature of deformation and the associated structures at stepovers between echelon strike-slip faults (see Ballance & Reading 1980, Biddle & Christie-Blick 1985). A few recent publications (e.g. Aydin & Nur 1982, 1985, Mann *et al.* 1983, Bahat 1984) provide extensive surveys of previously recognized stepovers, as well as a number of new ones, and describe their prominent features. Theoretical stress and displacement fields at stepovers were investigated by Segall & Pollard (1980), Rodgers (1980) and Mavko (1982). The effects of interaction between colinear strike-slip faults on stress drop, seismic moment and strain energy release were explored by Rudnicki & Kanamori (1981). However, the origin of echelon patterns of strike-slip faults and the reasons for their conspicuous geometry were essentially left untouched. This paper represents an effort to fill this gap by assessing the effects of interaction on the geometry of strike-slip faults. The enhancing and impeding effect of interaction on the propagation of closely spaced echelon faults was previously suggested by Aydin *et al.* (1985) and Ma *et al.* (1986). A similar mechanism was proposed for echelon extensional fractures by Pollard *et al.* (1982), Pollard & Aydin (1984) and Sempere & Macdonald (1986).

FIELD DATA

We use both existing data available in the literature and some new data that we collected in the field. In using the existing data, we were faced with two problems in quantifying the geometric characteristics of echelon strike-slip faults. First, the published maps lack a uniform accuracy. In dealing with the uniformity problem, we considered data from California (U.S.A.), Turkey and Israel. The data on faults from California come chiefly from geologists with the United States Geological Survey (Clark 1973, Wallace 1973, Sharp 1979), where strict mapping and publication guidelines and an internal review system assure uniformity. The data on the major faults in Turkey and Israel are obtained primarily from single authored documentary papers (e.g. Ketin 1969, Garfunkel 1981). Second, many faults or fault segments are linked by cross fractures, introducing a certain degree of ambiguity in the determination of individual strike-slip fault ends. In this case, we relied upon the interpretations by the original authors or compilers.

Figure 1 includes some of the strike-slip faults from California. These examples alone capture the dominant geometric features that are common to all the strike-slip faults that were used in this study. For the fault maps that were used for the entire data set in Table 1, the reader is referred to Aydin & Schultz (in press). In order to characterize the echelon nature of the faults, we measured the overlap ($2o$) and separation ($2s$) of echelon fault segments (Table 1, see Fig. 3b for the definition of geometric parameters), and plotted them against each other in Fig. 2. The measurement was straightforward for fault traces that are parallel. For those cases in which fault traces are curved or non-parallel, the chord length and average separation were taken as the overlap and separation, respectively. The log–log scale used for Fig. 2 makes it possible to compare measurements with a

* Present address: Geodynamics Branch, Code 621, NASA Goddard Space Flight Center, Greenbelt, MD 20771, U.S.A.

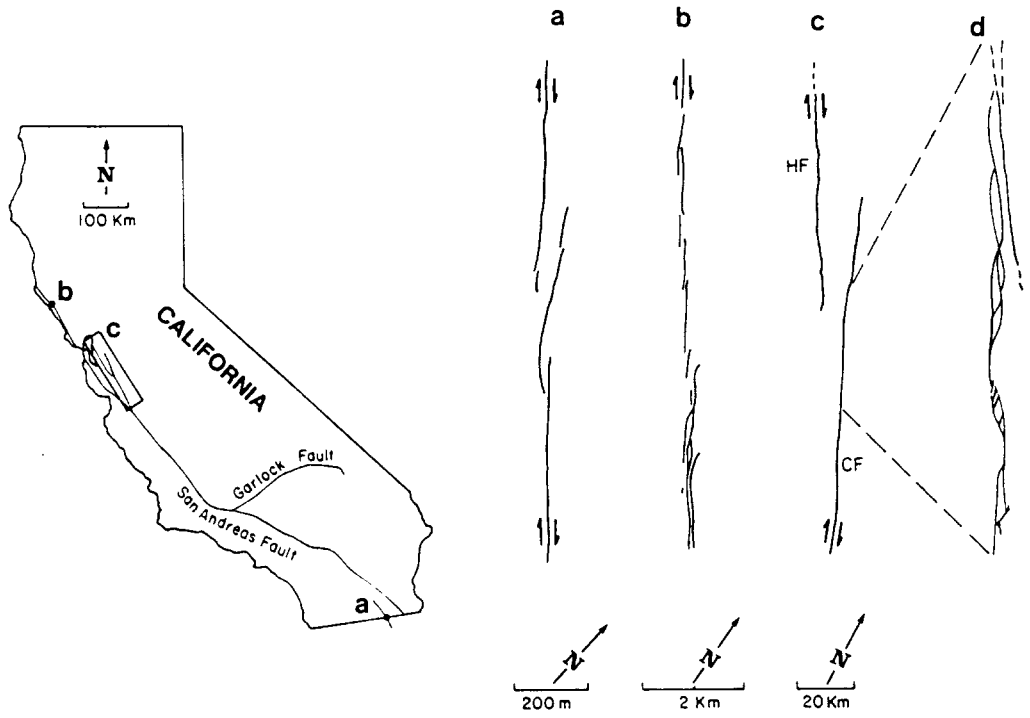

Fig. 1. Echelon steps along the San Andreas fault system. (a) Imperial fault (from Sharp 1979). (b) San Andreas Fault proper in northern California (from Wallace 1973, originally mapped by Brown & Wolfe 1972). (c) Hayward–Calaveras Fault (simplified from Aydin & Page 1984). (d) Central Calaveras Fault (from Aydin & Page unpublished fault map).

scale differential of several orders of magnitude, at the expense of an apparent compression of the spread of the data in the plot.

Figure 2 and Table 1 show the following features of the echelon arrays of the strike-slip fault systems. (1) The majority of adjacent faults overlap. Only about 10% of steps have underlap configuration (negative 2*o* in Table 1 and Fig. 2 inset), reflecting cases in which the inner fault tips do not pass each other. (2) The overlap is roughly proportional to the separation in a broad range

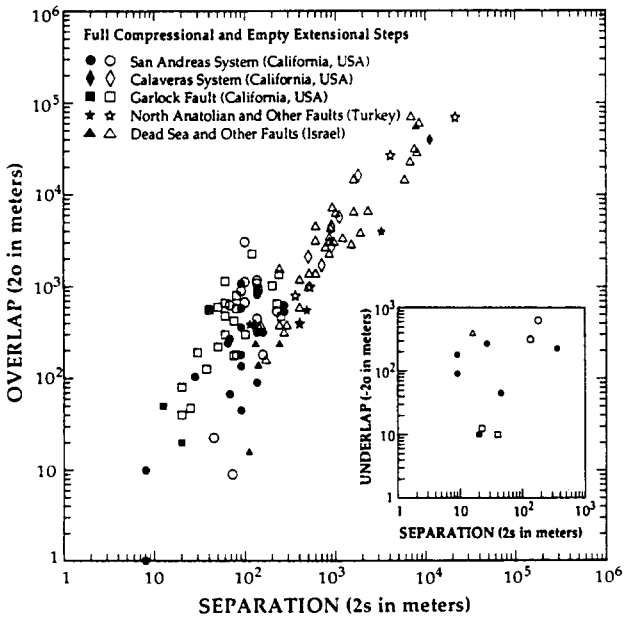

Fig. 2. Plot of overlap vs separation of echelon faults listed in Table 1. Inset shows underlap vs separation for those faults whose inner tips do not pass each other.

of scales (Fig. 2). There appears to be no consistent relationship between the underlaps and the corresponding separations (Fig. 2 inset). (3) The number of extensional steps or pull-aparts (the sense of displacement being the same as the sense of step) is more than that of compressional steps or push ups (the sense of displacement being the opposite of the sense of step). (4) The overlap–separation ratios for compressional steps (full symbols in Fig. 2) tend to be slightly smaller than those for extensional steps (empty symbols in Fig. 2). (5) Steps of various sizes occur along the same fault or fault strand (Fig. 1). (6) Large-scale echelon faults have smaller steps along the portions of the faults making the large steps. For example, the Calaveras Fault, which forms a large left step with the Hayward Fault (Fig. 1c), has several smaller steps (Fig. 1d). A similar situation occurs also in the Imperial Fault (Fig. 1a). Thus, the consistent overlap–separation ratios in all scales suggest that longer faults with larger separations do not feel smaller discontinuities along the individual faults.

The field data presented in Figs. 1 and 2 are compelling enough to conclude that echelon strike-slip faults tend to overlap slightly. Although the data are scattered, their approximately linear trend indicates that echelon fault patterns are self-similar to a first-order approximation. This generalization is consistent with that reached previously by Tchalenko (1970) that the geometries of shear zones in various scales are similar.

ANALYSIS

The persistence of the echelon pattern of strike-slip faults over a broad range of scales motivates an investi-

Table 1. Overlap–separation data

Fault system	Location	Displacement sense	Step sense	Overlap ($2o$) (m) underlap ($-2o$) (m)	Separation ($2s$) (m)	Reference
San Andreas		R	L	900.0	135.0	Wallace (1973)
		R	L	−90.0	9.0	
		R	L	810.0	135.0	
		R	L	45.0	90.0	
		R	L	540.0	270.0	
		R	L	−180.0	9.0	
		R	L	−90.0	9.0	
		R	L	−270.0	27.0	
		R	L	90.0	135.0	
		R	L	630.0	270.0	
		R	L	315.0	135.0	
		R	L	−225.0	360.0	
		R	R	−630.0	180.0	
		R	L	−45.0	45.0	
		R	L	585.0	90.0	
		R	L	67.5	67.5	
		R	L	180.0	90.0	
		R	L	270.0	67.5	
		R	L	135.0	90.0	
		R	L	315.0	157.5	
		R	R	900.0	90.0	
		R	R	630.0	67.5	
		R	R	1125.0	99.0	
		R	R	675.0	99.0	
		R	L	1080.0	90.0	
		R	R	22.5	45.0	
		R	R	3060.0	99.0	
		R	R	360.0	135.0	
		R	R	540.0	225.0	
		R	R	−315.0	135.0	
		R	R	180.0	157.5	
		R	L	360.0	90.0	
		R	R	9.0	72.0	
		R	R	1170.0	135.0	
		R	R	450.0	135.0	
		R	R	1080.0	135.0	
	Imperial Fault	R	L	240.0	64.0	Sharp (1979)
		R	L	10.0	8.0	
		R	L	1.0	8.0	
		R	L	104.0	28.0	
Calaveras	Hayward	R	L	39,900.0	11,200.0	Aydin & Page (1984)
		R	R	16,200.0	1800.0	Aydin & Page (unpublished map)
	Halls Valley	R	R	4500.0	900.0	
	San Felipe Valley	R	R	1700.0	700.0	
		R	R	5700.0	1100.0	
		R	R	2100.0	500.0	
	Coyote Lake	R	R	2700.0	900.0	
Garlock		L	L	300.0	100.0	This study
		L	L	580.0	80.0	
		L	L	480.0	60.0	
		L	L	180.0	80.0	
		L	L	220.0	50.0	
		L	R	20.0	20.0	
		L	L	1140.0	60.0	
		L	L	40.0	20.0	
		L	L	300.0	60.0	
		L	L	80.0	20.0	
		L	L	190.0	30.0	
		L	R	−10.0	20.0	
		L	R	580.0	40.0	
		L	L	660.0	60.0	
		L	L	1020.0	200.0	
		L	L	600.0	50.0	
		L	L	800.0	80.0	
		L	L	2260.0	120.0	
		L	L	560.0	40.0	
		L	L	920.0	140.0	
		L	L	−10.0	40.0	
	Christmas Canyon	L	L	1350.0	237.5	Clark (1973)
		L	L	425.0	75.0	
		L	R	50.0	12.5	

continued

Table 1. *Continued*

Fault system	Location	Displacement sense	Step sense	Overlap ($2o$) (m) underlap ($-2o$) (m)	Separation ($2s$) (m)	Reference
Garlock (*continued*)		L	L	−12.5	22.5	
		L	L	175.0	75.0	
		L	L	125.0	37.5	
		L	L	650.0	225.0	
		L	L	475.0	250.0	
		L	L	47.5	25.0	
Dead Sea	Arava Fault	L	L	385.0	290.0	Garfunkel *et al.* (1981)
		L	L	385.0	150.0	
		L	L	385.0	240.0	
		L	L	6730.0	2310.0	
		L	L	1400.0	510.0	
		L	L	7360.0	920.0	
		L	L	32,200.0	7600.0	
		L	L	3200.0	600.0	
		L	L	1200.0	400.0	
		L	L	1200.0	400.0	
		L	L	1000.0	500.0	
		L	L	3400.0	1200.0	
		L	L	1400.0	600.0	
		L	L	6400.0	1000.0	
		L	L	600.0	400.0	
		L	L	14,800.0	1600.0	
		L	L	4600.0	600.0	
	Hula Basin	L	L	23,200.0	6800.0	
		L	L	4400.0	880.0	
		L	L	14,700.0	5900.0	
		L	L	2900.0	1500.0	
		L	R	56,400.0	7880.0	
		L	L	3500.0	850.0	Garfunkel (1981)
		L	L	2700.0	770.0	
		L	L	3100.0	960.0	
		L	L	3900.0	1900.0	
		L	L	6600.0	1600.0	
		L	L	3100.0	850.0	
		L	L	2300.0	850.0	
	Gulf of Elat	L	L	61,600.0	8500.0	
		L	L	29,300.0	8090.0	
		L	L	72,400.0	6930.0	
		R	R	160.0	170.0	Ron & Eyal (1985)
		R	L	16.0	110.0	
		R	L	140.0	140.0	
		R	R	1580.0	240.0	
		L	R	240.0	240.0	
		L	R	240.0	130.0	
		L	L	320.0	270.0	
		L	L	−400.0	16.0	
North Anatolian	Yenice	R	R	400.0	400.0	Ketin (1969)
		R	L	400.0	400.0	
		R	L	560.0	480.0	
		R	R	800.0	360.0	
		R	R	1000.0	520.0	
	Kargi	R	R	27,000.0	4100.0	
	Erbaa	R	L	4000.0	3240.0	
		R	R	70,200.0	21,600.0	
	Kirsehir	R	L	390.0	130.0	
		R	L	390.0	113.0	

gation of the processes that may control the geometry of strike-slip faults. One of these processes is fault interaction, which undoubtedly occurs among nearby faults or fault segments (Segall & Pollard 1980). In order to assess the importance of fault interaction on the geometry of echelon strike-slip faults, we analyze the enhancing and impeding effect of interaction on the propagation of echelon faults. We use a special boundary element method called displacement discontinuity (Crouch 1976, 1979, Crouch & Starfield 1983), which is based on a solution for a single dislocation with constant displacement. We divide echelon faults into a number of boundary elements (Fig. 3), each of which has uniform slip. Slip on each element is driven by remote stresses (σ_1 and σ_3) and adjusted iteratively until shear and normal tractions (σ_s and σ_n, respectively) satisfy the prescribed boundary conditions; either frictionless or the Coulomb frictional slip criteria. Interaction between elements on nearby echelon faults is investigated by using an iterative solution procedure.

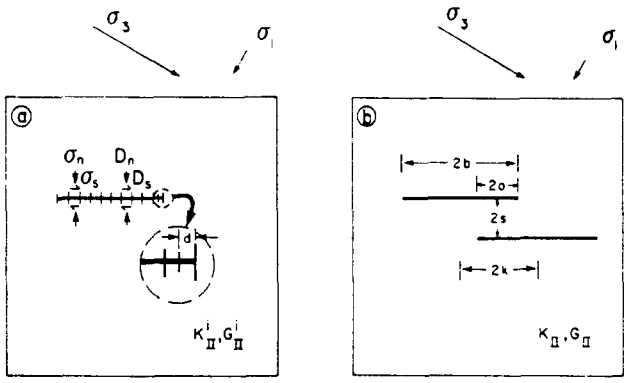

Fig. 3. Model parameters of echelon faults. Maximum and minimum remote principal stresses are σ_3 and σ_1, respectively. (a) Normal and shear components of boundary tractions (σ_n and σ_s) and displacement discontinuities (D_n and D_s) are shown on boundary elements k and j, respectively. The distance between the fault tip and the midpoint of the fault tip element is d. (b) Geometric parameters for echelon faults: fault length $2b$, center distance $2k$, overlap $2o$, separation $2s$.

Although many physical aspects of shear fracture propagation are not well understood, it is reasonable to assume that near-tip stress concentration plays an important role in fracture growth. For mode II fractures, the stress intensity factor (K^i_{II}) that characterizes the near-tip stresses for an isolated single fracture (Fig. 3a) is given in terms of the shear component of the displacement discontinuity, D_s, as

$$K^i_{II} = \frac{-\mu}{4\pi(1-\nu)}\left(\frac{2\pi}{d}\right)^{1/2} D_s$$

(Sempere & Macdonald 1986, Lin & Parmentier 1988, Schultz 1988), where d is the distance from fault tip to the midpoint of the nearest element (Fig. 3a), μ is the shear modulus and ν is the Poisson's ratio. D_n in Fig. 3(a) is the normal component of the displacement discontinuity, which is positive for opening and negative for closure. The propagation energy, G^i_{II}, which is the energy available for a unit growth of an isolated mode II fracture, is given by (Lawn & Wilshaw 1975)

$$G^i_{II} = \frac{(K^i_{II})^2(1-\nu)}{2\mu}.$$

Fault propagation energies at the inner tips of echelon faults are calculated for a suite of fault geometries. For each s/k (see Fig. 3b for the definition of center length, $2k$), fault lengths are increased incrementally to simulate growth of the faults. For each case, the values of G_{II} for echelon faults are normalized by those for an isolated single fault (G^i_{II}) in order to focus on only the effect of the interaction between echelon faults. For example, if $G_{II}/G^i_{II} = 1$, there is no interaction between the faults. On the other hand, ratios of $G_{II}/G^i_{II} \neq 1$ reflect fault interaction either enhancing (>1) or impeding (<1) the propagation of echelon faults. Shear modulus, μ, and Poisson's ratio, ν, have no effect on the change in the propagation energy due to fault interaction. Fault elements in the model are defined as thin zones with specific normal and shear stiffnesses. Especially useful is the normal stiffness, which can be so adjusted that the fault walls are prevented from physically interpenetrating

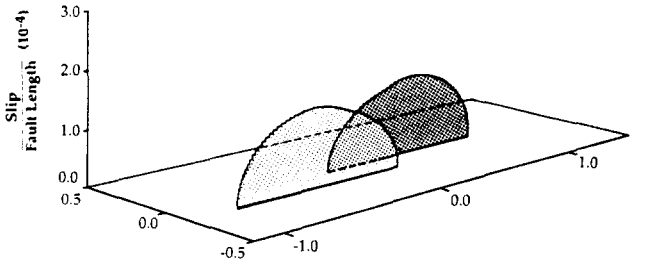

Fig. 4. Slip distribution along two overlapping echelon faults. Each fault is represented with 55 elements each with constant slip (displacement discontinuity). Remote principal stresses are compressive with magnitudes 5 and 1 MPa. Shear modulus and Poisson's ratio are arbitrarily chosen to be 10^4 MPa and 0.25, respectively.

(i.e. $D_n \geq 0$), which is a problem for echelon geometries with large overlaps under compressive remote stresses. We have set the stiffness ratio of fault zone material to surrounding rock at 10 to limit interpenetration. However, we have examined the role of relative values for fault zone stiffnesses on the interpenetration of fault surfaces and the degree of overlap. The remote stress state is defined by using a ratio of principal stresses of 5 with the maximum compressive stress inclined 30° to the faults. This ratio of the principal stresses is sufficient to produce slip everywhere along echelon faults for the highest value of friction coefficient in this study.

We have investigated a broad range of models, only three of which are considered in this paper. The first one assumes a frictionless fault zone in order to avoid nonlinearity introduced by the dependence of fault slip on normal stress. For this case the results from both extensional and compressional steps are about the same, so only the extensional case is presented. Figure 4 is a three-dimensional graph showing slip distribution along two echelon right-lateral faults with zero friction. Slip, which is constant on each element, is the highest near the centers of the faults and gradually decreases to zero at the fault tips. Figure 5 includes the curves of fault

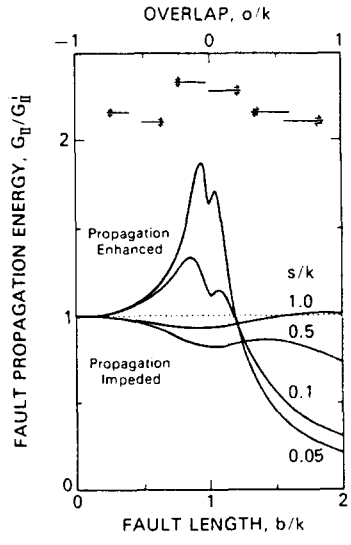

Fig. 5. Fault propagation energy for frictionless faults in extensional step normalized by that for an isolated fault. Fault interaction is stronger for relatively closely spaced echelon faults, whose propagation energies increase sharply as the inner tips approach each other and decrease after the inner tips pass each other to form a slightly overlapping step.

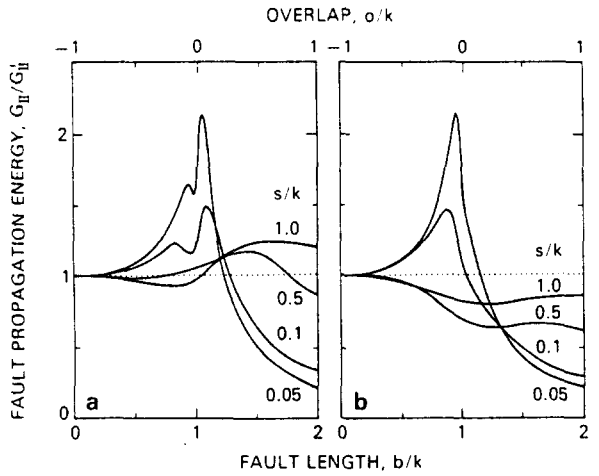

Fig. 6. Influence of step sense and friction on fault propagation energy. Friction coefficient $f = 0.6$. (a) Extensional step. (b) Compressional step. The effects of the interaction in both cases are similar to that of the frictionless case presented in Fig. 5. The drop of the propagation energy for overlapping fault configurations is more pronounced for compressional steps than for extensional steps.

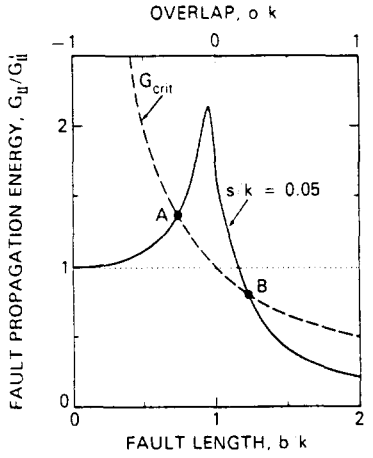

Fig. 7. Comparison of normalized fault propagation energy (G_{II}/G_{II}^i) to normalized critical propagation energy (G_{II}^c/G_{II}^i). For a hypothetical case, marked as G_{crit} in the figure, faults would start to propagate at A and terminate at B, producing an overlapping geometry of about $b/k = 1.25$.

propagation energy for four geometric cases ($s/k = 0.05$, 0.1, 0.5 and 1.0). The propagation energy for relatively closely spaced echelon faults ($s/k = 0.05$ and 0.1) increases as the inner fault tips approach each other (see the fault configurations illustrated at the top of the figure), and decreases sharply beyond zero overlap ($b/k = 1$). In contrast, the propagation energy for widely spaced echelon faults ($s/k > 1$) shows little change.

The second model includes two cases, extensional (Fig. 6a) and compressional (Fig. 6b) steps, using a Coulomb slip criterion with a friction coefficient of 0.6 (Byerlee 1978). In this model, the amount of slip (not shown) is, of course, less than that of the frictionless case in Fig. 4. In both compressional and extensional cases, the enhancing and impeding natures of fault interactions are generally similar to the frictionless fault cases. The difference between the compressional and the extensional cases is that the decrease of fault propagation energy for overlapped faults is much sharper for the compressional case.

Ideally, a fault would propagate when the propagation energy reaches a critical value G_{II}^c, which is dependent on material properties and the geometric parameters of a fault. We illustrate the propagation and termination of a pair of echelon faults with $s/k = 0.05$, using an arbitrarily chosen normalized critical propagation energy curve as shown in Fig. 7. Fault growth due to the interaction between the echelon faults will occur at the geometry corresponding to $b/k = 0.8$ (point A) and the growth will terminate when $b/k = 1.2$ (point B). Unfortunately, very little is known about the critical value of the mode II propagation energy for rocks. Hence, the arguments in this paper have to be rather qualitative. By noting that an increase (or decrease) in the fault propagation energy enhances (or impedes) the fault growth, the interaction between neighboring faults favors a slightly overlapped fault pattern. The exact amount of the overlap cannot be calculated at the present time. However, the forms of normalized fault propagation energy curves (Figs. 5 and 6), together with possible normalized critical fault propagation energy curves (for simplicity only one curve is shown in Fig. 7), suggest that amount of overlap (b/k) increases with amount of fault separation (s/k). Furthermore, the limit of separation for significant interaction appears to be on the order of the center distance ($s/k \sim 1.0$).

DISCUSSION AND SUMMARY

We have quantified the well-known observation that strike-slip faults the world over occur in echelon patterns with some overlap. The overlap is generally larger as the spacing of the neighboring faults increases. The results from our numerical analysis indicate that fault interaction enhances the growth of echelon faults as the inner tips pass each other and impedes their growth after some degree of overlap. Thus, we suggest that fault interaction is one of the processes responsible for the commonly-observed echelon geometry of strike-slip faults.

The frictionless and frictional slip criteria produce similar curves of fault propagation energy for the underlap configurations. Differences become pronounced as the amount of overlap increases. The frictionless case lies inbetween the extensional and the compressional cases, as expected from the role of fault-normal stresses on fault slip. The difference between the extensional and the compressional propagation energy curves may suggest greater overlaps for the extensional steps. Although not conclusive, the field data lend some support for this argument (see the generally lower ratios for the compressional steps, full symbols, in Fig. 2). A wide range of normal stiffness values for fault zones has been used to investigate the influence of normal stiffness on fault surface interpenetration and the amount of overlap. It has been found that high normal stiffnesses prevent the interpenetration. Normal stiffnesses lower

than that of the surrounding rock result in longer overlaps.

We have tested the influence of the orientation and magnitude of remote stresses on fault propagation energy due to fault interaction. Interestingly, we have found that as long as there is slip along the echelon faults the normalized propagation energy curves are essentially the same, regardless of remote stress state. However, it is likely that rock anisotropy and inhomogeneities have some influence on the geometry of interacting echelon faults. These possible effects have not been considered in this paper.

The results reported in this paper are relevant also to the self-similarity of pull apart basins and push up ranges (Aydin & Nur 1982) that form at extensional and compressional steps, respectively, along strike-slip faults. Although the length parameters for the basins and ranges are different (usually larger) than the overlap parameters of the strike-slip faults considered in this paper, the role of fault interaction is likely to be similar in the evolution of the geometry of pull apart basins and push up ranges. Our results are consistent with those of Ma *et al.* (1986), who used a perturbation method to determine the stability of echelon strike-slip faults.

Acknowledgements—This study has been supported in part by the U.S. Geological Survey Award No. 14-08-0001-G1084. R. A. Schultz gratefully acknowledges support from a David Ross Fellowship (Purdue University) and from a National Research Council-NASA Goddard Space Flight Center Resident Research Associateship. Discussions with D. Pollard, S. Nemat-Nasser, P. Segall, A. Nur and Y. Du were quite helpful. We are thankful for thoughtful comments by J. Andrews, P. Segall and an anonymous reviewer and for help by G. Ohlmacher for the production of some of the figures.

REFERENCES

Allen, C. R. 1981. The modern San Andreas Fault. In: *The Geotectonic Development of California* (edited by Ernst, W. G.). Prentice-Hall, Inc., Englewood Cliffs, New Jersey, 511–534.

Aydin, A. & Nur, A. 1982. Evolution of pull-apart basins and their scale independence. *Tectonics* **1**, 91–105.

Aydin, A. & Nur, A. 1985. The types and role of stepovers in strike-slip tectonics. In: *Strike-slip Deformation, Basin Formation, and Sedimentation* (edited by Biddle, K. T. & Christie-Blick, N.). *Spec. Publs Soc. econ. Paleont. Miner.* **37**, 35–44.

Aydin, A. & Page, B. M. 1984. Diverse Pliocene–Quaternary tectonics in a transform environment. *Bull. geol. Soc. Am.* **95**, 1303–1317.

Aydin, A. & Schultz, R. A. In press. The effect of fault interaction on the stability of echelon strike-slip faults. *U.S. geol. Surv. Open File Rep.*

Aydin, A., Schultz, R. A. & Pollard, D. D. 1985. Why do strike-slip faults overlap? (Abs.). *EOS (Trans. Am. Geophys. Un.)* **66**, 1067–1068.

Bahat, D. 1984. New aspects of rhomb structures. *J. Struct. Geol.* **5**, 591–601.

Ballance, P. F. & Reading, H. G. (editors) 1980. *Sedimentation in Oblique-slip Mobile Zones. Spec. Publs Int. Ass. Sediment* **4**.

Biddle, K. T. & Christie-Blick, N. (editors) 1985. *Strike-slip Deformation, Basin Formation, and Sedimentation. Spec. Publs Soc. econ. Paleont. Miner.* **37**.

Bonilla, M. G. 1979. Historic faulting-map patterns, relation to subsurface faulting and relation to pre-existing faults. In: *Proc. Conf. VIII: Analysis of Actual Fault Zones in Bedrock. U.S. geol. Surv. Open File Rep.* **79-1239**, 36–65.

Brown, R. D. & Wolfe, E. W. 1972. Map showing recently active breaks along the San Andreas fault between Point Delgada and Bolinas Bay, California. *U.S. geol. Surv. Misc. Geol. Invest. Map* I-692.

Byerlee, J. 1978. Friction of rocks. *Pure & Appl. Geophys.* **116**, 615–626.

Clark, M. M. 1973. Map showing recently active breaks along the Garlock and associated faults, California. *U.S. geol. Surv. Misc. Geol. Invest. Map* I-741.

Crouch, S. L. 1976. Solution to plane elasticity problems by the displacement discontinuity method. *Int. J. Num. Meth. Engng* **10**, 301–343.

Crouch, S. L. 1979. Computer simulation of mining in faulted ground. *J. S. Afr. Instn Min. Metall.* **79**, 159–173.

Crouch, S. L. & Starfield, A. M. 1983. *Boundary Element Methods in Solid Mechanics*. George Allen & Unwin, London.

Garfunkel, Z. 1981. Internal structure of the Dead Sea leaky transform (rift) in relation to plate kinematics. *Tectonophysics* **80**, 81–108.

Garfunkel, Z., Zak, I. & Freund, R. 1981. Active faulting in the Dead Sea rift. *Tectonophysics* **80**, 1–26.

Ketin, I. 1969. Kuzey Anadolu fayi hakkinda (in Turkish and German). *Maden Tetkik Arama Enstitüsü Dergisi* **72**, 1–27.

Lawn, B. R. & Wilshaw, T. R. 1975. *Fracture of Brittle Solids*. Cambridge University Press, Cambridge.

Lin, J. & Parmentier, E. M. 1988. Quasistatic propagation of a normal fault: A fracture mechanics model. *J. Struct. Geol.* **10**, 249–262.

Ma, J., Du, Y. & Liu, L. 1986. The instability of en-echelon cracks and its precursors. *J. Phys. Earth* **34**, Suppl., S141–S157.

Mann, P., Hempton, M. R., Bradley, D. C. & Burke, K. 1983. Development of pull-apart basins. *J. Geol.* **91**, 529–554.

Mavko, G. M. 1982. Fault interaction near Hollister, California. *J. geophys. Res.* **87**, 7807–7816.

Pollard, D. D., Segal, P. & Delaney, P. T. 1982. Formation and interpretation of dilatant echelon cracks. *Bull. geol. Soc. Am.* **93**, 1291–1303.

Pollard, D. D. & Aydin, A. 1984. Propagation and linkage of oceanic ridge segments. *J. geophys. Res.* **89**, 10,017–10,028.

Rodgers, D. A. 1980. Analysis of pull-apart basin development produced by en-echelon strike-slip faults. In: *Sedimentation in Oblique-slip Mobile Zones* (edited by Ballance, P. F. & Reading, H. G.). *Spec. Publs Int. Ass. Sediment.* **4**, 27–41.

Ron, H. & Eyal, Y. 1985. Intraplate deformation by block rotation and mesostructures along the Dead Sea transform, northern Israel. *Tectonics* **4**, 85–105.

Rudnicki, J. W. & Kanamori, H. 1981. Effects of fault interaction on moment, stress drop, and strain energy release. *J. geophys. Res.* **86**, 1785–1793.

Schultz, R. A. 1988. Stress intensity factors for curved cracks obtained with the displacement discontinuity method. *Int. J. Fract.* **37**, R31–R34.

Schultz, R. A. In press. Strike-slip faulting in the ridged plains of Mars. NASA MEVTV Workshop on *Tectonic Features on Mars* (Abs.), Richland, Washington, 19–21 April 1989.

Segall, P. & Pollard, D. D. 1980. Mechanics of discontinuous faults. *J. geophys. Res.* **85**, 4337–4350.

Sempere, J.-C. & Macdonald, K. C. 1986. Overlapping spreading centers: implications from crack growth simulation by the displacement discontinuity method. *Tectonics* **5**, 151–163.

Sharp, R. V. 1979. The implication of surficial strike-slip fault patterns for simplification and widening with depth. In: *Proc. Conf. VIII: Analysis of Actual Fault Zones in Bedrock. U.S. geol. Surv. Open File Rep.* **79-1239**.

Tchalenko, J. S. 1970. Similarities between shear zones of different magnitudes. *Bull. geol. Soc. Am.* **81**, 1625–1640.

Wallace, R. E. 1973. Surface fracture patterns along the San Andreas Fault. In: *Proc. Conf. on Tectonic Problems of the San Andreas Fault System* (edited by Kovach, R. L. & Nur, A.). School of Earth Sciences, Stanford University, Stanford, California, 248–250.